Miner Deposita (2014) 49:843–860
DOI 10.1007/s00126-014-0513-8

ARTICLE

Cassiterite LA-MC-ICP-MS U/Pb and muscovite $^{40}Ar/^{39}Ar$ dating of tin deposits in the Tengchong-Lianghe tin district, NW Yunnan, China

Xiao-Cui Chen · Rui-Zhong Hu · Xian-Wu Bi · Hui-Min Li · Jiang-Bo Lan · Cheng-Hai Zhao · Jing-Jing Zhu

Received: 27 October 2013 / Accepted: 1 March 2014 / Published online: 22 April 2014

Abstract The Tengchong-Lianghe tin district in northwestern Yunnan, China, is an important tin mineralization area in the Sanjiang Tethyan Metallogenic Domain. There are three N–S trending granite belts in the Tengchong-Lianghe area, with emplacement ages ranging from Early Cretaceous to Late Cretaceous and Early Cenozoic. Tin mineralization is spatially associated with these granitic rocks. However, the petrogenetic link between the tin deposits and the host granites is not clear because of the lack of age data for the tin mineralization. We investigate the possibility of direct dating of cassiterite from three typical tin deposits in the Tengchong-Lianghe tin district, using laser ablation multicollector inductively coupled plasma mass spectrometry (LA-MC-ICP-MS). In situ LA-MC-ICP-MS dating of seven cassiterite samples from the Lailishan (LLS-1 and LLS-2), Xiaolonghe (XLH, WDS, DSP, and HJS), and Tieyaoshan (TYS) tin deposits yielded well-defined $^{206}Pb/^{207}Pb$–$^{238}U/^{207}Pb$ isochron ages. To assess the accuracy of the in situ U/Pb dating of cassiterite, $^{40}Ar/^{39}Ar$ dating of coexisting muscovite (in samples LLS-1, DSP, and TYS) was also performed. The cassiterite in situ U/Pb ages (47.4±2.0, 71.9±2.3, and 119.3±1.7 Ma, respectively) are in excellent agreement with the coexisting muscovite $^{40}Ar/^{39}Ar$ ages (48.4±0.3, 71.9±1.4, and 122.4±0.7 Ma, respectively). The U/Pb ages of cassiterite combined with the $^{40}Ar/^{39}Ar$ ages of muscovite indicate that there are three tin mineralization events in this district: the Lailishan tin deposit at 47.4±2.0 to 52±2.7 Ma, the Xiaolonghe tin deposit at 71.6±2.4 to 3.9±2.0 Ma, and the Tieyaoshan tin deposit at 119.3±1.7 to 122.5±0.7 Ma. These ages are highly consistent with the zircon U/Pb ages of the host granites. It is su.ggested that the Cretaceous tin mineralization might have taken place in a subduction environment, while the Early Tertiary tin metallogenesis was in a postcollisional geodynamic setting.

Keywords Cassiterite · LA-MC-ICP-MS U/Pb dating · Muscovite $^{40}Ar/^{39}Ar$ dating · Tin deposits · Granite · Yunnan Province · China

Editorial handling: B. Lehmann

X.-C. Chen · R.-Z. Hu · X.-W. Bi · J.-B. Lan · C.-H. Zhao · J.-J. Zhu
State Key Laboratory of Ore Deposits Geochemistry, Institute of Geochemistry, Chinese Academy of Sciences, Guiyang 550005, China

X.-C. Chen · C.-H. Zhao
University of Chinese Academy of Sciences, Beijing 100049, China

H.-M. Li
Tianjin Institute of Geology and Mineral Resources, Tianjin 300170, People's Republic of China

R.-Z. Hu (✉)
Institute of Geochemistry, Chinese Academy of Sciences, 46 Guanshui Road, Guiyang 550002, People's Republic of China
e-mail: huruizhong@vip.gyig.ac.cn

Introduction

Determining the age of mineral deposits is critical for understanding ore genesis and related geological processes. However, direct age constraints on ore formation are often difficult because of the lack of suitable mineral phases that can be unequivocally linked to mineralization. Apart from approaches such as K/Ar, Ar/Ar, and Rb/Sr dating of gangue and ore-related alteration minerals, there were several attempts to obtain isotopic ages of ore minerals with remarkable progress over the past decade, e.g., Sm/Nd dating of scheelite and wolframite (Bell et al. 1989; Kempe et al. 2001; Peng et al. 2003) and Re/Os dating of molybdenite (Mao et al. 1999; Stein et al. 2001; Yuan et al. 2012). Direct U/Pb dating of rutile (TiO_2) has been widely accepted (Birch et al. 2007; Kooijman et al. 2010; Li et al. 2003; Schandl et al. 1990;

Zack et al. 2011). Cassiterite (SnO_2) and rutile belong to the rutile group ($M^{4+}O_2$); therefore, cassiterite should offer the same advantages as rutile for direct dating of mineral deposits. Cassiterite is the main ore phase in most tin deposits, often contains significant amounts of U and has the ability to preserve U and radiogenic Pb (Gulson and Jones 1992; Yuan et al. 2008; Zhang et al. 2011). In recent years, laser ablation–multicollector–inductively coupled plasma–mass spectrometry (LA-MC-ICP-MS), which enables the simultaneous in situ analysis of U/Pb isotopes and trace elements, has been employed for dating zircon and other U-bearing accessory phases such as baddeleyite, monazite, titanite, rutile, allanite, perovskite, xenotime, and eudialyte (Cox and Wilton 2006; Horn et al. 2000; Horstwood et al. 2003; Schmidberger et al. 2005; Simonetti et al. 2006; Simonetti and Neal 2010; Valeriano et al. 2011; Wu et al. 2010; Zhou and Li 2008). LA-MC-ICP-MS offers several advantages over conventional methods, including simple sample preparation procedures, measurement of isotopic ratios at high spatial resolution (5–40 μm), rapid analysis, and low cost (Simonetti et al. 2006; Simonetti and Neal 2010; Smith et al. 2005; Storey et al. 2007; Willigers et al. 2002; Zhang and Schärer 1996). There have been some attempts to evaluate the U/Pb isotope systematics of cassiterite as a geochronometer by isotope dilution thermal ionization mass spectrometry (ID-TIMS) (Gulson and Jones 1992; Liu et al. 2007; Yuan et al. 2008, 2011). Nonetheless, to date, there have been only a few attempts to employ in situ LA-MC-ICP-MS U/Pb dating of cassiterite for the direct dating of tin mineralization (Li et al. 2013; Yuan et al. 2011). Thus, the universal use of cassiterite for direct dating by in situ LA-MC-ICP-MS needs to be verified with more examples.

The Tengchong-Lianghe tin district in western Yunnan is an important tin mineralization area in the Sanjiang Tethyan Metallogenic Domain (STMD) of Southwest China (Hou et al. 2007). The STMD is an important part of the Tethyan metallogenic megaprovince, which is one of the three Phanerozoic metallogenic megaprovinces in the world (i.e., Tethyan, Paleo-Asian, Circum-Pacific) (Hou et al. 2007). Understanding the genesis of tin deposits in the Tengchong-Lianghe tin district is critical for understanding metallogenesis in the STMD and the Tethyan metallogenic megaprovince. There are three N–S trending granite belts in the Tengchong-Lianghe area, with emplacement ages ranging from Early Cretaceous, to Late Cretaceous and Early Cenozoic (Chen 1987; Li et al. 2012a, b; Xu et al. 2011; Yang et al. 2009). Tin mineralization is spatially associated with these granitic rocks. Previous studies were focussed on the geology, fluid inclusions, stable isotopes and mineral chemistry of the tin deposits in this district (Shi et al. 1991; Tang 1992a, b; Xu et al. 2010). However, the genetic link between the tin deposits and the spatially related granites is unclear, due to the lack of age data for the tin mineralization.

The aims of this study are (1) to elucidate the genesis of tin deposits in the region; and (2) to evaluate the U/Pb isotope system in cassiterite for direct dating by in situ LA-MC-ICP-MS. For this purpose, we collected seven cassiterite samples according to ore type and distribution from three typical tin deposits (Lailishan, Xiaolonghe, and Tieyaoshan) for in situ LA-MC-ICP-MS U/Pb dating. Moreover, we used $^{40}Ar/^{39}Ar$ dating of muscovite coexisting with cassiterite for assessing the in situ U/Pb age data of cassiterite.

Regional geology

The Tibetan plateau comprises several terranes such as the Songpan–Ganzi, Qiangtang, and Lhasa blocks (Fig. 1a). The Yalung Tsangpo suture separates the Indian plate and Lhasa block. The latter is separated from the Qiangtang block by the Bangong-Nujiang suture zone which formed during the late Jurassic and early Cretaceous due to the closure of the Meso-Tethys (Shi et al. 2008; Yin and Harrison 2000). The India-Yalung Zangbo Ocean (Neo-Tethys Ocean) opened in about Middle Jurassic; its northward subduction resulted in the formation of the Gangdese magmatic arc during the Cretaceous. At ~65 Ma, the India–Eurasia collision (Neo-Tethys Ocean closure) formed Yalung Tsangpo suture and created the Tibetan plateau (Hou et al. 2007; Mo et al. 2008). The STMD is tectonically located in the southeastern segment of the Tibetan plateau and the eastern margin of the Yalung Tsangpo or India–Eurasia suture (Hou et al. 2007).

The Tengchong-Lianghe tin district, located in the southwestern part of the STMD, and the eastern segment of the Gangdese magmatic arc (Fig. 1a, b), is the most important tin district in the STMD. It consists of two large tin deposits (Lailishan and Xiaolonghe, more than 50,000 tonnes Sn), five medium-sized tin deposits (30,000 to 50,000 tonnes Sn), and nearly a hundred mineralized localities. There are three N–S trending granite belts in the Tengchong-Lianghe area (Fig. 1b), namely, the Early Tertiary granites, the Late Cretaceous granites, and the Early Cretaceous granites (Hou et al. 2007). Moreover, there is a younging trend oblique to the regional geological strike, from NE to SW. The Early Cretaceous granitic rocks are divided into three major units (Diantan, Mingguang and Qipanshi), and have zircon U/Pb ages varying from 118.8±4.2 to 127.1±0.96 Ma (Cong et al. 2010; Li et al. 2012b; Xu et al. 2011). The granitic rocks are mainly granodiorite and biotite granite, and are mostly mineralized. The medium-sized Tieyaoshan tin deposit occurs in the Qipanshi granite unit (Fig. 1b). The Late Cretaceous granitic rocks include two major granite units (Xiaolonghe and Yunfengshan) with zircon U/Pb ages of 67.8±1.4 to 76.0±1.0 Ma (Xu et al. 2011). The large Xiaolonghe tin deposit is associated with ore-bearing biotite granite in the Xiaolonghe granite unit (Fig. 1b). The Early Tertiary granites consist of the

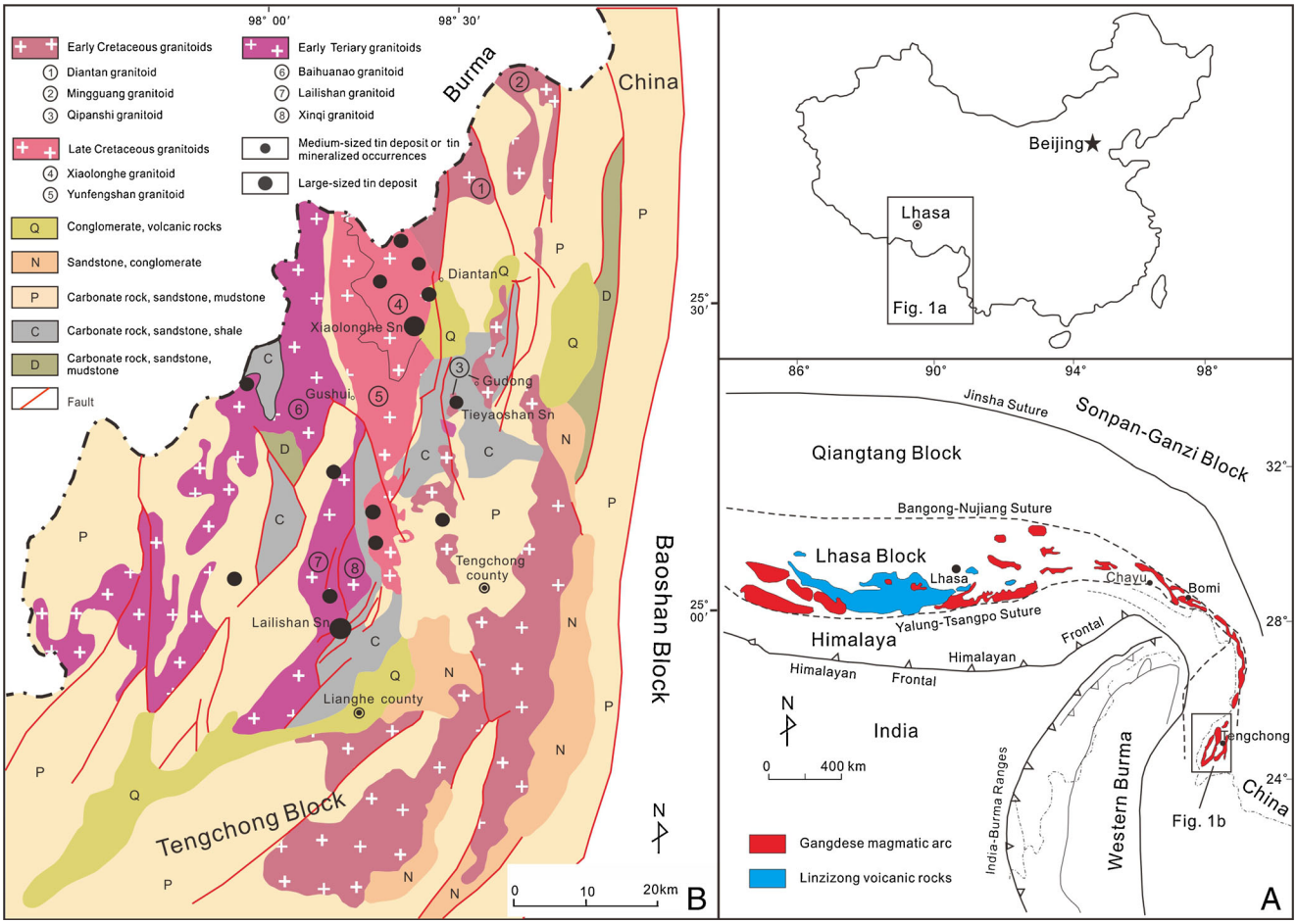

Fig. 1 Sketch map showing (**a**) the tectonic framework of the Tibetan Plateau (Hou et al. 2007; Tang 1992) and (**b**) the distribution of magmatic rocks as well as tin deposits in the Tengchong-Lianghe tin district (Chen 1987; Hou et al. 2007)

Xinqi, Lailishan, and Baihuanao granitic units, and have zircon U/Pb ages ranging from 52.1±0.8 to 56.3±1.1 Ma (Xu et al. 2011). The large Lailishan tin deposit is spatially related with the Lailishan granitic unit (Fig. 1b).

Deposit geology

Samples were collected from two large tin deposits (Lailishan and Xiaolonghe) and the medium-sized Tieyaoshan deposit. The Lailishan tin deposit has a Sn reserve of approximately 58,000 tonnes with an average Sn grade of 0.66 % (Liu et al. 2005). Ore bodies mainly occur in the outer contact zones of the Early Tertiary granite, or the fractured zones surrounding the granitic intrusion (Fig. 2a). The spatially related granite is predominantly biotite granite and the wall rocks are mainly Carboniferous carbonate rocks, sandstones, and shales. In this deposit, the main ore bodies are V-57, V-36, and V-10, and only the latter is presently exploited. Three ore types can be identified based on mineral association and occurrence: greisen, quartz vein, and skarn. The greisen-type ores mainly consist of cassiterite, quartz, muscovite/sericite, and pyrite. Cassiterite is coarse-grained with a grain size of up to hundreds of micrometers; some cassiterite grains typically have short prismatic and bipyramidal shape (Fig. 3a_1, a_2). The quartz vein-type ores consist of cassiterite, quartz, topaz, muscovite, and fluorite. They are the richest mineralization style with a grade of up to 60 % for some ores (Fig. 3b_1, b_2), and account for 30–50 % of the reserves. Cassiterite and muscovite in the ore have a radial shape (Fig. 3b_2). The skarn-type ores are of minor importance, and the typical skarn mineral is garnet. The hydrothermal alteration of the Lailishan tin deposit mainly includes carbonatization, skarnitization, and silicification.

The Xiaolonghe tin deposit occurs in the Late Cretaceous granite and is the largest tin deposit in the Tengchong-Lianghe tin district with Sn reserves of approximately 65,600 tonnes (Liu et al. 2005). The ore bodies vary greatly in size, ranging in length from 30 to 300 m and in thickness from 1 to 20 m. There are four ore clusters (Xiaolonghe, Wandanshan, Dasongpo, and Huangjiashan; Fig. 2b). The Xiaolonghe and Wandanshan ore clusters are dominated by quartz vein-type ore bodies, occurring in granite or the surrounding rocks (Fig. 2b). Quartz and cassiterite are the main minerals in this

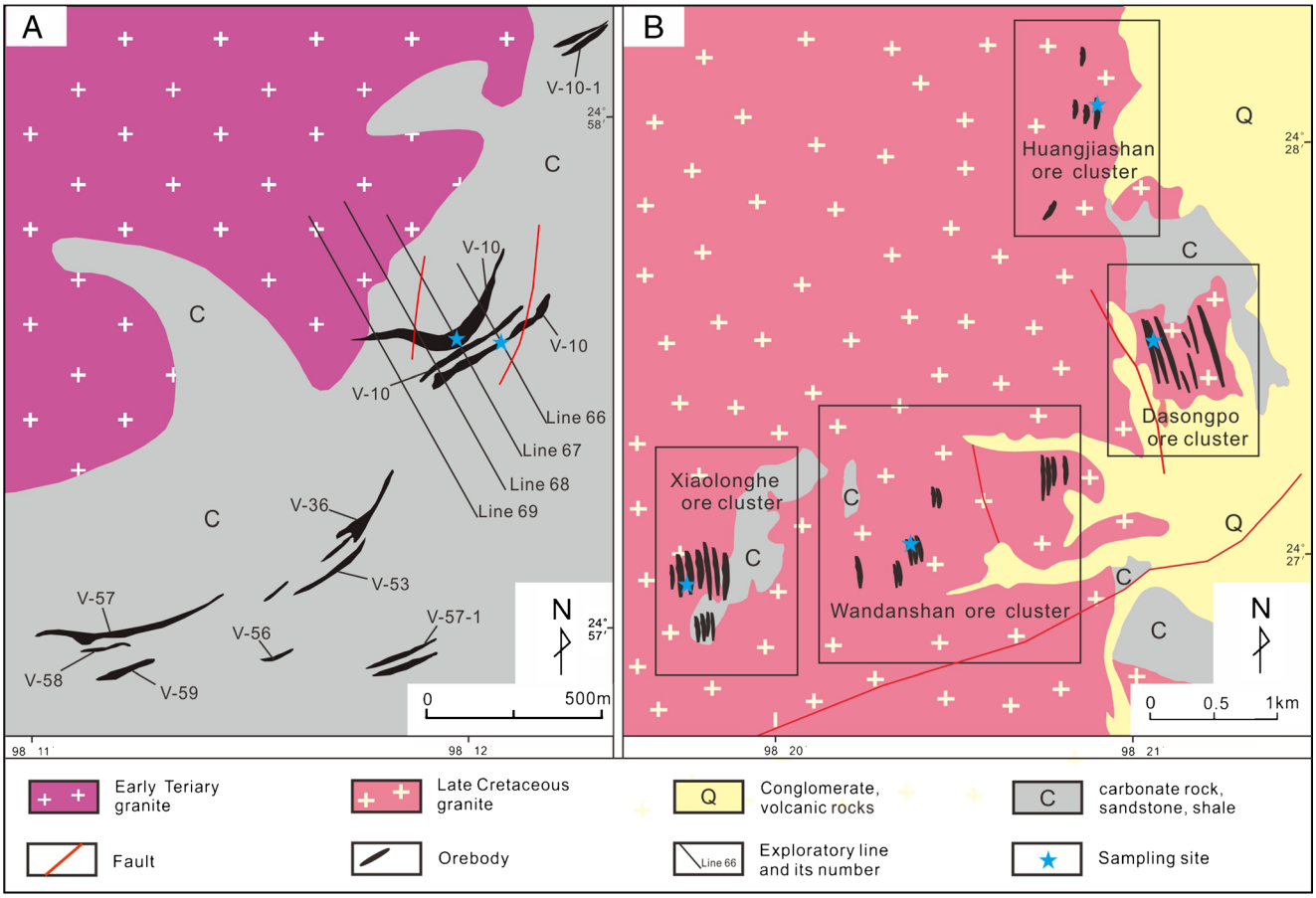

Fig. 2 Simplified geological map of the (**a**) Lailishan and (**b**) Xiaolonghe tin deposits

type (Fig. 3c_1, c_2). The Dasongpo and Huangjiashan ore clusters are dominated by greisen-type ores in granite and mainly consist of cassiterite, muscovite, quartz, and pyrite (Fig. 3d_1, d_2).

The medium-sized Tieyaoshan tin deposit occurs in the Early Cretaceous granite. Tin mineralization occurs in biotite granites and is dominated by greisen-type ores (Fig. 3e_1, e_2). The ore minerals in this deposit are mainly cassiterite and pyrite, and the gangue minerals are primarily quartz, fluorite, muscovite, and calcite.

Sampling and analytical methods

Sample collection and preparation

Seven cassiterite samples were collected from the Tengchong-Lianghe tin district and analyzed in two batches for LA-MC-ICP-MS U/Pb dating. The first batch of samples (LLS-1, LLS-2) was collected from the V-10 ore body of the Lailishan deposit. LLS-1 is a quartz vein-type ore, and LLS-2 is a greisen-type ore (Fig. 2a). The second batch of five samples was collected from four ore clusters of the Xiaolonghe deposit (XLH, quartz vein-type ore; WDS, quartz vein-type ore; DSP, greisen-type ore; HJS, greisen-type ore; Fig. 2b) and the Tieyaoshan deposit (TYS, greisen-type ore). All samples were crushed to 40–60 mesh, and the cassiterite grains were separated using heavy liquids and magnetic separation techniques and were then mounted on epoxy disks. The disks were polished, carbon coated, and examined by reflected light microscopy, backscattered electron (BSE) imaging, and cathodoluminescence (CL) imaging to characterize the texture of cassiterite. Prior to U/Pb dating, samples LLS-1, XLH, and TYS were prepared for electron microprobe analysis at the State Key Laboratory of Ore Deposit Geochemistry (SKLODG), Institute of Geochemistry, Chinese Academy of Sciences. The microphotographs and BSE images were also taken in the same lab. The CL images were taken using a JSM-6510 at Geoanalysis Institute Co., Ltd. in Beijing.

In situ LA-MC-ICP-MS dating of cassiterite

The in situ LA-MC-ICP-MS U/Pb dating of cassiterite was performed at the Tianjin Institute of Geology and Mineral Resources. Laser sampling was performed using an ESI UP193FX ArF excimer laser ablation system with a wavelength of 193 nm, a pulse width of ~4 ns, an adjustable spot

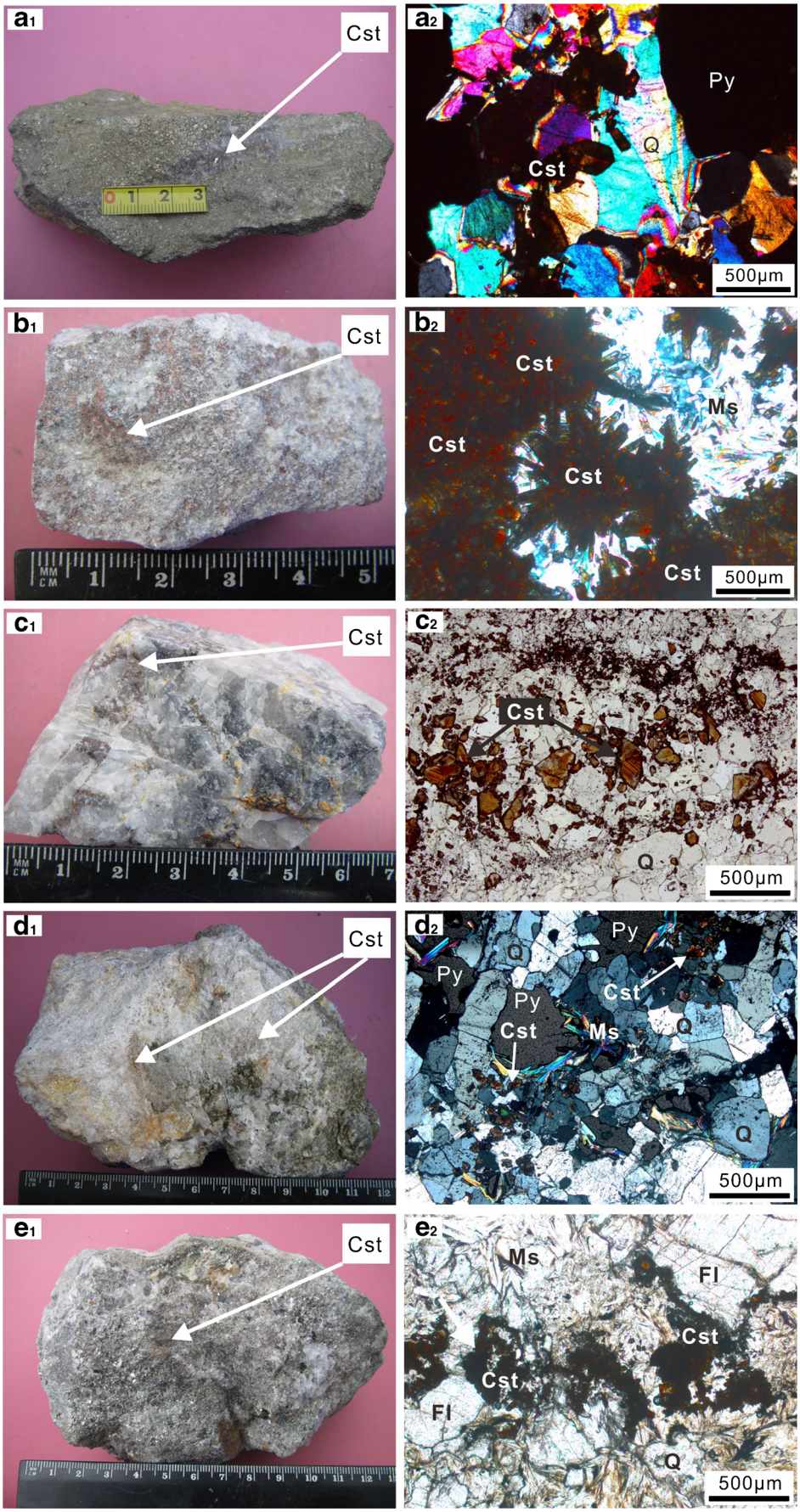

Fig. 3 Photographs of the main ore types from the three tin deposits. a_1 and a_2 greisen-type ore and b_1 and b_2 quartz vein-type ore from the Lailishan tin deposit; c_1 and c_2 quartz vein-type ore and d_1 and d_2 greisen-type ore from the Xiaolonghe tin deposit; e_1 and e_2 greisen-type ore from the Tieyaoshan tin deposit. *Cst* cassiterite; *Py* pyrite; *Ms* muscovite; *Q* quartz; *Fl* fluorite

size of 2–150 μm, a continuously adjustable laser pulse frequency of 1–200 Hz, and an energy density of approximately 15 J/cm^2. An MC–ICPMS (Neptune, Thermo Fisher Scientific) instrument equipped with nine Faraday cups (one axial and eight off-axis) and four ion counters was employed to acquire ion signal intensities. The double-focusing MC-ICP-MS with zoom optics can measure isotope ratios with a relative mass difference of up to 17 %. Helium, which effectively reduces the degree of U/Pb within-run fractionation during single-spot ablation analyses and typically results in increased sensitivity, was employed as a carrier gas (Horn et al. 2000; Li et al. 2010; Yuan et al. 2011). Details of instrument parameters and conditions are illustrated in Cui et al. (2012), Yuan et al. (2011) and Zhou et al. (2012).

To date, there are no globally accepted cassiterite standards for U/Pb dating. To simultaneously correct instrument mass bias and laser-induced U/Pb fractionation, a cassiterite (AY-4) sample was used as the in-house external standard. The AY-4 sample was collected from the giant Furong tin deposit in Hunan Province, South China. Precise $^{40}Ar/^{39}Ar$ ages of hydrothermal muscovite, phlogopite, and hornblende constrain the ages (156.1±0.4 to 160.1±0.9 Ma) of the Furong tin deposit (Mao et al. 2004; Peng et al. 2007). The U/Pb age of the standard cassiterite (AY-4) was established by ID-TIMS as 158.2±0.4 Ma (Yuan et al. 2011) and is in excellent agreement with the $^{40}Ar/^{39}Ar$ ages.

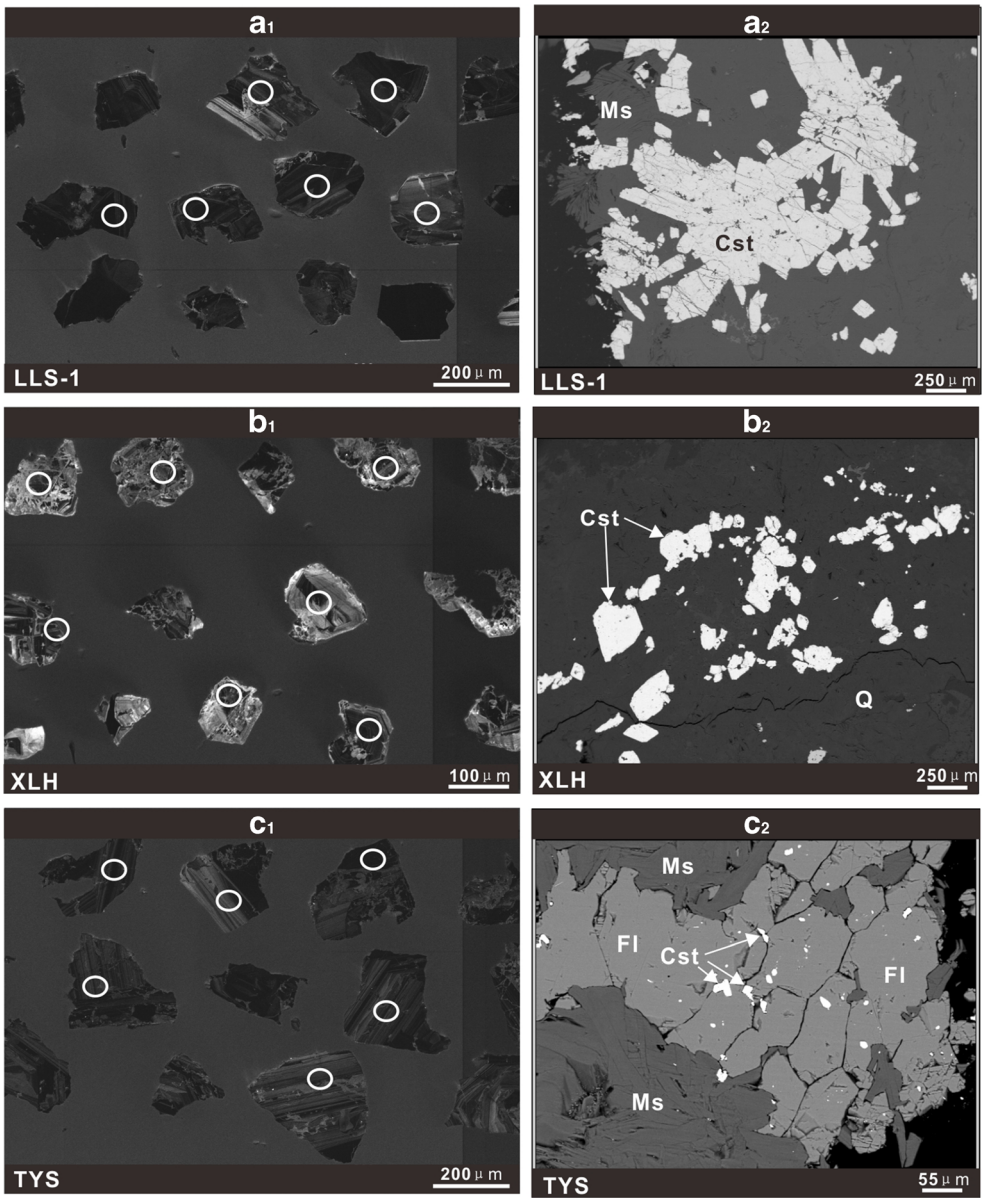

Fig. 4 Cathodoluminescence (CL) (a_1, b_1, c_1)and backscattered electron (BSE) (a_2, b_2, c_2) images of cassiterite (LLS- 1 from the Lailishan tin deposit; XLH from the Xiaolonghe tin deposit; TYS from the Tieyaoshan tin deposit). The ellipses indicate the in situ LAMC- ICP-MS analysis spots for U/Pb isotopes. *Cst* cassiterite; *Ms* muscovite; *Q* quartz; *Fl* fluorite

Table 1 Electron microprobe analyses (wt%) of cassiterite (LLS-2 from the Lailishan tin deposit, DSP from the Xiaolonghe tin deposit, and TYS from the Tieyaoshan tin deposit)

Sample	MgO	Al_2O_3	SiO_2	TiO_2	Cr_2O_3	MnO	FeO	SnO_2	Total
LLS-2-1	0.34	0.06			0.01		1.21	97.54	99.16
LLS-2-2	0.36	0.03	0.04			0.02	0.29	97.78	98.53
LLS-2-3	0.39	0.07			0.01	0.01	0.76	98.46	99.71
LLS-2-4	0.36	0.01			0.02	0.04	0.91	97.97	99.30
LLS-2-5	0.40	0.03					1.09	98.10	99.61
LLS-2-6	0.37					0.03	0.10	98.63	99.13
LLS-2-7	0.38	0.01		0.07		0.01	0.05	99.08	99.61
LLS-2-8	0.38			0.06	0.01	0.02	0.20	98.91	99.58
LLS-2-9	0.38	0.06	0.04		0.04	0.01	0.84	98.03	99.38
LLS-2-10	0.39	0.06	0.04				0.61	97.92	99.02
LLS-2-11	0.47	0.07	0.02	0.08			0.21	98.04	98.88
LLS-2-12	0.39	0.02	0.01				0.82	98.22	99.46
LLS-2-13	0.38	0.06	0.01		0.04	0.05	0.38	97.64	98.55
LLS-2-14	0.35	0.08			0.02		0.63	98.63	99.71
LLS-2-15	0.34	0.00					0.01	98.75	99.10
LLS-2-16	0.36						0.07	98.51	98.94
XLH-1	0.33	0.05	0.08	0.03	0.01		0.07	98.19	98.75
XLH-2	0.39	0.01	0.04	0.01	0.01	0.01	0.32	98.28	99.06
XLH-3	0.36				0.01	0.01	0.08	99.20	99.65
XLH-4	0.40	0.01	0.07	0.02	0.02	0.01	0.12	98.62	99.26
XLH-5	0.33	0.01	0.01	0.01			0.29	98.81	99.46
XLH-6	0.47	0.04	0.04	0.07	0.03		0.13	97.95	98.73
XLH-7	0.36	0.02	0.03		0.01	0.01	0.56	98.65	99.64
XLH-8	0.53	0.01	0.09	0.07	0.01	0.03	0.06	98.29	99.10
XLH-9	0.44	0.01	0.04				0.27	98.39	99.16
XLH-10	0.37		0.00		0.02		0.34	97.93	98.66
XLH-11	0.34	0.02					0.16	98.55	99.07
XLH-12	0.34	0.01					0.13	97.98	98.47
XLH-13	0.39	0.03		0.18	0.03	0.02	0.32	98.47	99.43
XLH-14	0.34	0.01				0.01	0.23	98.26	98.85
XLH-15	0.38	0.02	0.01	0.10		0.02	0.46	98.44	99.43
XLH-16	0.35	0.01			0.01	0.02	0.35	99.13	99.88
XLH-17	0.38	0.01		0.05	0.01		0.11	99.13	99.70
XLH-18	0.43	0.01	0.01				0.35	97.77	98.56
XLH-19	0.36	0.01	0.04	0.04			0.17	99.07	99.67
TYS-1	0.35				0.01	0.02	0.07	98.33	98.77
TYS-2	0.47	0.03	0.04	0.21	0.01	0.01	0.31	98.07	99.13
TYS-3	0.37	0.07	0.03	0.78	0.01	0.02	0.34	98.21	99.83
TYS-4	0.36			0.76		0.01	0.32	98.15	99.60
TYS-5	0.32	0.02		0.22			0.49	98.21	99.26
TYS-6	0.41	0.02		0.47	0.01		0.16	98.03	99.09
TYS-7	0.31	0.03		0.78	0.02		0.20	98.18	99.51
TYS-8	0.34			0.19	0.01		0.06	98.53	99.12
TYS-9	0.37			0.58		0.01	0.20	98.25	99.40
TYS-10	0.37	0.04		0.22	0.02		0.40	98.54	99.59
TYS-11	0.37			0.54	0.01		0.37	98.48	99.77
TYS-12	0.31	0.01		0.68		0.02	0.14	97.94	99.10
TYS-13	0.34	0.01		0.11			0.37	97.90	98.73

Table 1 (continued)

Sample	MgO	Al_2O_3	SiO_2	TiO_2	Cr_2O_3	MnO	FeO	SnO_2	Total
TYS-14	0.40	0.01		0.43	0.01	0.01	0.21	98.49	99.55
TYS-15	0.41	0.02	0.03	0.57	0.02	0.01	0.49	97.81	99.35
TYS-16	0.35	0.04		0.18	0.01	0.01	0.52	98.21	99.31
TYS-17	0.36	0.01		0.46			0.04	99.01	99.87
TYS-18	0.32	0.03		0.10			0.35	98.44	99.23

Before the analysis, the sample surface was cleaned with ethanol to eliminate possible contamination. For epoxy grain mounts, the cassiterite standard and unknown cassiterite grains were placed together so that the standard could be frequently analyzed without opening the ablation cell. The selection of areas for isotope analysis was based on the size, morphology, and internal texture of the cassiterite characterized by reflected and transmitted light microscopy and CL imaging. All spot analyses were made on clean grains, or clean parts of the grains. The laser was focused to produce ablation pits ranging in diameter from 35 to 50 μm with a laser pulse rate of 8–10 Hz. Every 4–5, sample analyses were followed by a suite analyses of external cassiterite standard. The analytical procedures were the same as those previously used for cassiterite in the same laboratory (Li et al. 2013; Yuan et al. 2011). All the $^{207}Pb/^{206}Pb$ and $^{206}Pb/^{238}U$ values for the unknown samples were corrected using the cassiterite external standard, and the ages were calculated using Isoplot (Ludwig 1997, 2001).

$^{40}Ar/^{39}Ar$ dating of muscovite

To assess the accuracy and precision of the in situ LA-MC-ICP-MS U/Pb dating of cassiterite, we also performed $^{40}Ar/^{39}Ar$ dating of muscovite grains coexisting with the cassiterite grains from the LLS-1, DSP, and TYS samples. The sample was crushed and sieved in 40–60 mesh fractions; the muscovite crystals were selected by conventional winnowing and then by handpicking under a binocular microscope. The muscovite grains were wrapped in aluminum foil and irradiated in the nuclear reactor (the swimming pool reactor) at the Chinese Institute of Atomic Energy, Beijing. $^{40}Ar/^{39}Ar$ step-heating with a double-vacuum Ta resistance furnace was carried out according to set temperature. The released gas was purified with two Zr–Al getters, and argon isotopes were analyzed with an MM5400 mass spectrometer at the State Key Laboratory of Lithospheric Evolution, Institute of Geology and Geophysics, Chinese Academy of Sciences. The decay constant of ^{40}K used in the calculation for $^{40}Ar/^{39}Ar$ age is 5.543×10^{-10} a^{-1} (Steiger and Jäger 1977). Additional details about the analytical procedures are described by Mao et al. (2006) and Wang et al. (2006).

Results

Microscopic characteristics and chemical composition of cassiterite

The cassiterite crystals are light to dark brown, mostly euhedral to subhedral, and 10 to 100 μm in length (Figs. 3 and 4). Some coarse-grained cassiterite crystals have short prismatic or bipyramidal shape (Fig. 3b_2). The CL images clearly show oscillatory zoning, and the BSE images illustrate that cassiterite has higher luminance than other minerals (Fig. 4).

Major oxide data for the LLS-2, XLH, and TYS samples are listed in Table 1. Cassiterite is mainly composed of SnO_2 with an average Sn value of 98.3 wt%. The main impurities include Fe, Mg, and to a lesser extent, Al, Si, Ti, and Mn. All cassiterite grains have relatively uniform compositions of SnO_2 (97.5–99.2 wt%) and MgO (0.31–0.47 wt%). The color of cassiterite depends on the Fe content (Peng and He 1985). Dark cassiterite grains of the greisen-type ore samples (LLS-2 and TYS) from Lailishan and Tieyaoshan tin deposits (Fig. 3a_1, a_2 and e_1, e_2) have a higher average Fe content of 0.51 and 0.45 wt%, respectively. The light brown (Fig. 3c_1, c_2) cassiterite of the quartz vein-type ore sample (XLH) from the Xiaolonghe tin deposit has a relatively low Fe content with an average of 0.24 wt%.

U/Pb ages of cassiterite

The U/Pb data for the samples of the first batch (AY-4, LLS-1, and LLS-2) are summarized in Table 2 and illustrated in Fig. 5. The external standard (AY-4) yielded an isochron age of 160.3±3.9 Ma, which is consistent with the "standard" age of 158.2±0.4 Ma within error. This indicates that the data likely represent true values. The quartz vein-type sample (LLS-1) yielded an isochron age of 47.4±2.0 Ma (2σ, MSWD = 1.9) and the greisen-type sample (LLS-2) yielded an isochron age of 52.0±2.7 Ma (2σ, MSWD = 0.98).

The U/Pb data for the samples of the second batch (AY-4, XLH, WDS, DSP, HJS, and TYS) are listed in Table 3 and

illustrated in Fig. 6. There is a deviation between the measured data and the "standard" age of the external standard (AY-4). The large range of $^{206}Pb/^{207}Pb$ and $^{238}U/^{207}Pb$ ratios yielded well-defined isochron ages. The external standard (AY-4) yielded an isochron age of 144.1±2.8 Ma; therefore, we applied a correction value (J = measured value $_{(144.1)}$/ "standard" value $_{(158.2)}$) of 0.91. The corrected ratios of the quartz vein-type ore sample (XLH) from the Xiaolonghe ore cluster yielded an isochron age of 71.6±2.4 Ma (2σ, MSWD = 1.6). The quartz vein-type ore sample (WDS) from the Wandanshan ore cluster yielded a corrected isochron age of 72.8±1.8 Ma (2σ, MSWD = 0.72). The greisen-type ore

Table 2 U–Pb isotopic data for cassiterite from the first batch sample (AY-4 in-house external standard and LLS from the Lailishan tin deposit)

AY-4				LLS-1				LLS-2			
$^{238}U/^{207}Pb$	Error (%)	$^{206}Pb/^{207}Pb$	Error (%)	$^{238}U/^{207}Pb$	Error (%)	$^{206}Pb/^{207}Pb$	Error (%)	$^{238}U/^{207}Pb$	Error (%)	$^{206}Pb/^{207}Pb$	Error (%)
42.76	6.82	1.74	3.15	101.26	1.57	1.93	1.33	85.41	4.93	1.90	4.11
54.90	5.88	2.12	4.95	113.41	2.56	2.05	2.10	24.28	1.33	1.31	0.93
560.02	4.55	14.99	2.31	47.23	1.67	1.55	1.34	10.18	1.55	1.26	1.14
93.94	4.56	2.95	2.58	42.67	1.54	1.50	0.85	6.93	2.71	1.21	2.04
125.99	4.89	4.02	2.89	85.42	1.96	1.81	1.42	80.01	4.54	1.83	3.62
143.93	5.22	4.41	4.03	28.80	0.66	1.40	0.66	19.25	1.76	1.32	1.01
238.96	3.56	7.00	1.76	82.83	1.73	1.82	1.65	19.89	1.27	1.35	1.28
186.63	6.78	5.55	3.47	70.31	2.67	1.69	1.27	20.73	1.57	1.31	0.64
55.84	7.55	2.29	3.62	33.59	0.98	1.46	0.51	9.98	1.85	1.25	1.38
459.00	3.02	12.03	2.67	80.73	1.78	1.77	1.41	4.03	1.52	1.19	0.50
272.98	7.74	7.61	6.62	59.40	1.25	1.61	0.93	37.34	2.72	1.46	1.63
260.37	5.04	6.90	4.86	82.09	1.82	1.79	1.15	15.64	1.71	1.28	0.72
60.26	2.34	2.58	1.56	27.32	1.26	1.37	0.56	8.44	1.54	1.24	1.15
70.08	7.41	2.63	4.99	25.66	0.96	1.38	0.53	51.11	2.83	1.56	1.69
123.04	6.15	3.90	5.25	18.40	3.21	1.32	0.55	46.06	2.59	1.54	1.63
174.96	4.94	5.27	3.93	24.45	2.94	1.34	0.81	77.33	1.96	1.79	1.78
415.77	5.38	11.27	3.65	57.89	1.56	1.62	1.23	91.52	4.70	1.89	3.22
196.68	5.79	5.84	2.87	58.59	1.20	1.61	0.95	19.51	1.87	1.32	0.49
150.93	4.10	4.37	3.35	27.44	1.05	1.39	0.45	29.87	3.18	1.40	1.81
164.93	4.75	4.62	3.98	128.94	2.01	2.18	1.86	24.13	2.56	1.34	1.41
213.02	4.36	6.41	2.55	48.62	1.91	1.55	0.84	21.89	3.58	1.37	1.79
54.91	5.94	2.42	2.81	43.04	0.75	1.47	0.54	28.27	2.23	1.41	2.03
186.96	10.15	5.18	9.13	59.90	1.11	1.59	0.77	107.73	3.16	2.02	2.95
235.98	3.97	7.11	2.65	17.95	1.95	1.32	0.41	40.61	3.05	1.52	1.78
291.71	6.83	8.32	5.07	21.80	0.99	1.34	0.36	18.41	3.70	1.32	0.50
98.01	6.08	3.23	4.58	66.85	1.51	1.68	1.18	10.52	3.15	1.24	1.32
460.01	4.40	12.68	3.40	89.72	1.98	1.86	1.38	69.77	3.39	1.76	2.58
35.19	7.86	1.49	3.15	59.87	1.25	1.63	0.84	11.43	1.04	1.24	0.86
192.01	3.15	5.40	1.96	59.45	2.65	1.66	1.86	35.35	1.63	1.43	1.01
142.83	6.10	4.32	4.73	48.73	2.11	1.60	1.36	8.92	1.70	1.21	1.42
150.84	3.65	4.39	3.29					18.47	2.42	1.29	1.86
136.04	5.96	4.03	3.90								
238.33	7.69	6.50	3.82								
256.05	6.72	6.86	5.59								
164.08	7.38	4.64	5.80								
237.06	4.58	6.96	2.34								
59.84	7.45	2.42	5.24								
595.77	3.69	15.87	2.00								
46.38	3.82	1.92	3.01								

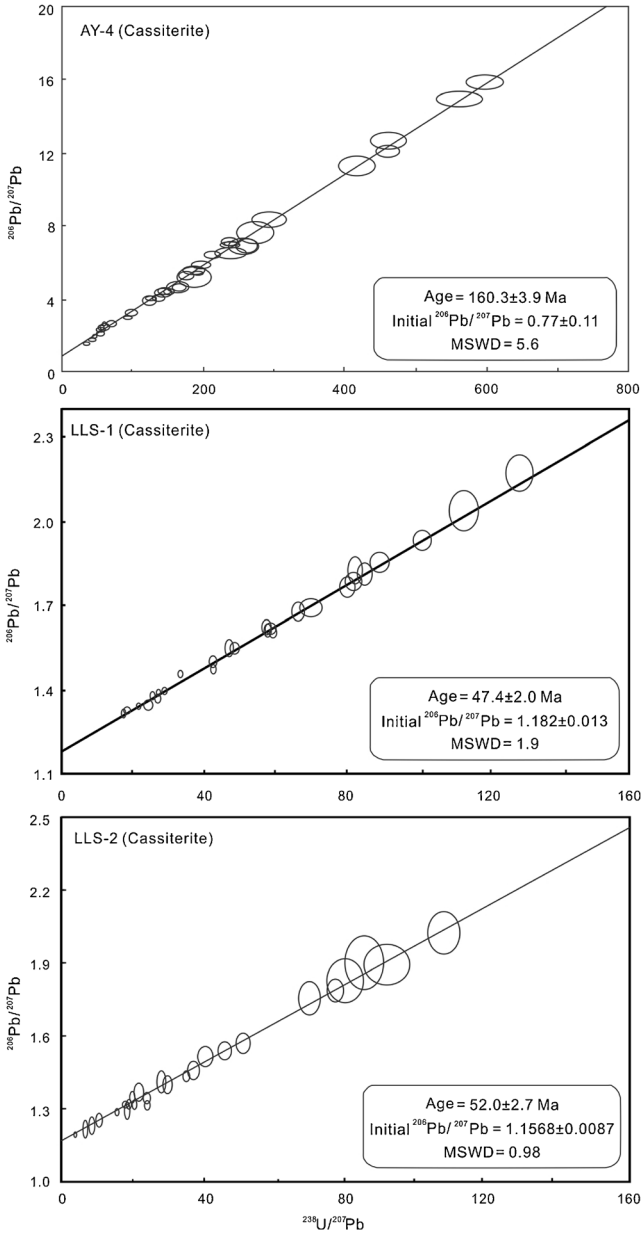

Fig. 5 $^{238}U/^{207}Pb$–$^{206}Pb/^{207}Pb$ isochron diagram for cassiterite in the samples of the first batch (Lailishan tin deposit)

sample (DSP) from the Dasongpo ore cluster yielded a corrected isochron age of 71.9±2.3 Ma (2σ, MSWD = 1.8). The greisen-type ore sample (HJS) of the Huangjiashan ore cluster yielded a corrected isochron age of 73.9±2.0 Ma (2σ, MSWD = 1.2). In situ LA-MC-ICP-MS dating of cassiterite from four samples obtained from the Xiaolonghe tin deposit yielded ages between 71.6±2.4 and 73.9±2.0 Ma. The corrected ratios of the greisen-type ore sample (TYS) from the Tieyaoshan tin deposit yielded an isochron age of 119.3 ±1.7 Ma (2σ, MSWD = 0.43).

$^{40}Ar/^{39}Ar$ ages of muscovite

The $^{40}Ar/^{39}Ar$ step-heating data of muscovite grains from the same ore samples (LLS-1, DSP, and TYS) are shown in Table 4. The LLS-1 sample from the Lailishan tin deposit yielded a plateau in the temperature interval 900–1,180 °C, with 9 out of 14 steps accounting for 74.5 % of the total ^{39}Ar released and MSWD of 1.31. The plateau age is 48.4±0.3 Ma, and the isochron age calculated for the same plateau steps is 48.4±0.3 Ma (Fig. 7). Sample DSP yielded a plateau in the temperature interval 780–1,100 °C, with 8 out of 12 steps accounting for 93.2 % of the total ^{39}Ar released. The plateau age was 71.9±0.5 Ma, and the isochron age calculated for the same plateau steps was 71.9±1.4 Ma (Fig. 7). Sample TYS exhibited a plateau in the temperature interval 840–1,120 °C, with 10 out of 15 steps accounting for 96.9 % of the total ^{39}Ar released. The plateau age was 122.5±0.7 Ma and the isochron age calculated for the same plateau steps was 122.4±0.7 Ma (Fig. 7). These ages are identical with our U/Pb ages (47.4±2.0, 71.9±2.3, and 119.3±1.7 Ma) of cassiterite from the same samples.

Discussion

Evaluation of in situ LA-MC-ICP-MS U/Pb dating of cassiterite

Different matrix and crystal structures between external standards and unknown samples could lead to mass bias and U/Pb fractionation. We chose a well-dated cassiterite sample (AY-4) as an external standard during our in situ LA-MC-ICP-MS U/Pb dating to eliminate the matrix effect. Typically, the isotopic composition of Pb is corrected using ^{204}Pb. However, in this study, the ^{204}Pb signal was low with interference from ^{204}Hg in the Ar gas, and consequently, it was not precisely measured. Therefore, ^{207}Pb and the isochron method are used to correct common Pb (Andersen 2002). Fortunately, the large range of $^{206}Pb/^{207}Pb$ ratios in cassiterite yielded well-defined $^{206}Pb/^{207}Pb$–$^{238}U/^{207}Pb$ isochron ages.

Samples of the first batch yielded data with a good linear relation; furthermore, the isochron age (160.3±3.9 Ma) of the external standard (AY-4) is concordant with the "standard" age (158.2±0.4) within error. This indicates that the ages of samples LLS-1 and LLS-2 are likely true values. The $^{40}Ar/^{39}Ar$ age (48.4±0.3 Ma) of coexisting muscovite is identical with the U/Pb age (47.4±2.0 Ma) of cassiterite from the same sample (LLS-1), which further supports these U–Pb ages of cassiterite. For the samples of the second batch, we used the correction value (J = measured value $_{(144.1)}$/"true value" $_{(158)}$) of 0.91 calculated using the external standard (AY-4) for

Table 3 U–Pb isotopic data for cassiterite from the second batch samples (AY-4 in-house external standard; XLH, WDS, DSP, and HJS from the Xiaolonghe tin deposit; and TYS from the Tieyaoshan tin deposit)

	$^{238}U/^{207}Pb$	Error (2 %)	$^{206}Pb/^{207}Pb$	Error (2 %)
AY-4-2	449.94	5.64	10.92	5.36
	55.07	6.37	2.38	3.22
	187.05	9.48	5.24	8.18
	257.56	11.72	6.89	10.59
	97.67	7.64	3.32	5.15
	144.27	4.69	4.39	3.79
	752.04	3.12	17.75	3.08
	143.44	5.38	4.26	4.02
	56.84	6.69	2.42	4.28
	34.38	4.07	1.92	3.17
	259.10	6.31	6.92	5.77
	64.08	8.28	2.63	5.41
	122.81	5.59	3.85	4.44
	175.21	5.23	5.05	4.81
	236.56	3.75	6.08	2.90
	56.30	8.16	2.35	4.17
	151.24	3.80	4.36	3.22
	165.12	5.60	4.62	4.45
	26.76	7.28	1.74	2.41
	44.01	6.87	2.11	3.23
	163.81	8.03	4.65	6.49
	472.71	5.58	11.06	5.08
	126.39	5.06	3.93	3.84
	202.10	9.22	5.41	7.53
	15.19	14.86	1.49	3.15
	191.90	2.96	5.44	2.40
	570.29	4.23	13.31	4.04
	150.84	3.65	4.39	3.29
	135.65	6.61	4.04	4.99
	236.40	4.16	7.07	3.94
	292.13	7.26	8.31	6.47
	112.65	11.10	3.31	10.06
	459.40	2.12	12.04	1.96
	273.39	12.24	7.56	11.09
	662.17	5.60	16.80	5.16
	789.89	2.83	19.17	2.78
	1068.34	1.87	25.16	1.83
XLH	64.05	1.65	1.90	0.92
	2.61	2.73	1.21	0.26
	8.66	1.38	1.27	0.59
	2.90	2.32	1.21	0.40
	28.93	2.66	1.50	2.03
	39.76	2.74	1.62	1.11
	2.79	4.75	1.21	1.55
	47.44	5.17	1.74	1.84
	61.88	3.46	1.89	2.08
	3.68	4.11	1.24	0.61
	22.08	3.96	1.43	1.01
	31.67	6.12	1.55	1.95
	23.93	2.21	1.45	0.81
	36.08	2.48	1.57	0.97
	45.57	4.16	1.71	1.73
	36.30	3.47	1.59	1.29
	53.16	2.32	1.79	1.17
	44.36	4.85	1.66	1.60
	26.08	2.98	1.47	0.97
	52.97	2.03	1.76	1.00
DSP	28.08	1.81	1.50	0.66
	54.36	2.10	1.80	1.18
	20.73	1.53	1.39	0.55
	8.26	1.89	1.27	0.25
	29.23	2.51	1.48	1.09
	19.51	3.35	1.38	1.30
	102.63	3.53	2.28	2.52
	22.82	3.14	1.43	1.71
	36.60	2.47	1.59	1.29
	30.08	3.18	1.53	1.74
	22.16	2.68	1.41	1.66
	33.50	3.07	1.56	1.90
	7.52	1.93	1.26	0.50
	86.16	3.65	2.17	2.77
	21.75	3.40	1.43	0.95
	3.09	1.49	1.21	0.13
	6.90	2.39	1.25	0.30
	45.30	2.42	1.69	1.32
	11.61	5.81	1.31	1.40
	60.78	2.59	1.86	1.56
	42.55	3.68	1.63	2.34
	14.17	3.26	1.34	2.38
	25.62	1.96	1.48	1.23
	37.00	3.68	1.58	2.19
	80.54	4.98	2.06	2.98
	54.85	3.34	1.82	2.48
	48.86	3.19	1.73	2.49
	37.17	3.33	1.57	1.87
	39.29	4.91	1.61	2.18
	40.15	6.25	1.63	2.10
WDS	7.62	2.59	1.27	0.52
	20.49	4.04	1.41	0.68
	66.39	5.78	1.94	2.85
	8.01	3.79	1.28	0.95
	31.97	6.19	1.53	4.25
	23.78	4.67	1.46	1.83
	201.10	7.32	3.46	5.26
	27.26	3.85	1.49	1.12
	13.49	6.88	1.34	3.75

Table 3 (continued)

	$^{238}U/^{207}Pb$	Error (2 %)	$^{206}Pb/^{207}Pb$	Error (2 %)
	6.90	3.02	1.27	1.16
	0.66	3.06	1.19	0.10
	2.04	3.49	1.21	0.14
	69.28	7.16	2.00	4.69
	37.68	2.12	1.60	0.77
	26.57	4.01	1.48	1.18
	26.56	2.39	1.49	1.55
	39.27	3.31	1.66	3.00
	23.86	8.75	1.45	1.72
	3.37	3.84	1.22	0.29
	80.13	8.26	2.15	5.11
	42.18	7.78	1.68	3.40
	56.03	4.33	1.82	1.75
	30.23	2.10	1.52	0.65
	17.08	3.48	1.42	2.50
	38.46	9.23	1.60	2.94
	28.17	4.07	1.49	1.50
	143.37	5.19	2.81	3.69
HJS	56.71	6.36	1.84	3.58
	59.44	3.34	1.88	2.62
	7.69	5.72	1.27	0.41
	9.05	9.12	1.34	2.81
	31.24	4.52	1.54	1.27
	38.26	13.77	1.61	3.86
	7.31	5.70	1.28	0.51
	16.64	3.72	1.38	0.77
	15.60	2.47	1.36	0.71
	17.18	3.25	1.39	0.54
	11.51	5.87	1.31	0.72
	54.64	5.57	1.81	2.38
	14.86	9.13	1.36	1.33
	17.87	11.05	1.41	1.84
	13.99	8.26	1.36	1.45
	71.70	11.01	2.03	5.23
	44.40	2.87	1.70	1.56
	15.94	6.78	1.40	1.91
	8.30	3.68	1.32	2.20
	143.30	5.74	2.81	3.52
	22.43	6.79	1.44	1.22
	15.44	8.50	1.37	1.85
	19.20	10.13	1.41	1.86
	52.50	2.62	1.80	1.28
	46.46	6.50	1.75	2.76
	7.54	5.78	1.28	0.47
TYS	233.56	4.17	5.49	3.63
	90.11	4.68	2.89	3.23
	144.64	4.18	3.85	3.11
	15.27	5.80	1.48	1.29
	218.19	4.02	5.27	3.20
	153.94	3.08	4.05	2.64
	259.34	5.08	6.05	4.61
	124.78	7.28	3.58	5.93
	117.19	4.20	3.44	3.43
	99.29	5.64	3.08	4.38
	42.06	4.90	2.06	2.52
	380.85	10.98	8.43	10.77
	173.14	5.79	4.48	5.09
	78.16	8.84	2.71	6.00
	54.17	3.21	2.24	2.46
	102.86	4.22	3.14	3.45
	87.03	4.69	2.81	3.28
	142.46	3.98	3.91	3.09
	506.72	4.29	10.73	4.08
	413.83	8.00	9.02	7.61
	168.37	3.37	4.31	2.84
	584.89	7.59	12.20	7.22
	112.38	5.45	3.32	4.22
	160.18	2.81	4.14	2.18
	179.95	6.34	4.64	5.18

correcting the deviation between the measured and "true" isotopic ratios. The corrected isotopic ratios of cassiterite from the four samples from the Xiaolonghe tin deposit yielded "true" ages within a narrow range from 71.6±2.4 to 73.9 ±2.0 Ma, and the greisen-type ore sample (TYS) from the Tieyaoshan tin deposit yielded a "true" age of 119.3±1.7 Ma. The $^{40}Ar/^{39}Ar$ ages (71.9 Ma and 122.4 Ma) of coexisting muscovite are in good agreement with the U/Pb ages (71.9 ±2.3 Ma and 119.3±1.7 Ma) of cassiterite in the same samples (DSP and TYS) from these two deposits. This firmly reinforces the accuracy estimates of the in situ LA-MC-ICP-MS dating of cassiterite. Furthermore, the data strongly demonstrate that in situ LA-MC-ICP-MS U/Pb dating of cassiterite could be employed for direct dating of tin mineralization events, especially for tin deposits lacking suitable minerals for other dating techniques.

Implications for the genesis of tin deposits in the Tengchong-Lianghe tin district

The U/Pb ages of cassiterite combined with the $^{40}Ar/^{39}Ar$ ages of muscovite provide tight constraints on the timing of tin mineralization in the Tengchong-Lianghe tin district. These ages indicate that there are three tin mineralization events in this district: the Lailishan tin deposit at 47.4±2.0 to 52 ±2.7 Ma, the Xiaolonghe tin deposit at 71.6±2.4 to 73.9 ±2.0 Ma, and the Tieyaoshan tin deposit at 119.3±1.7 to

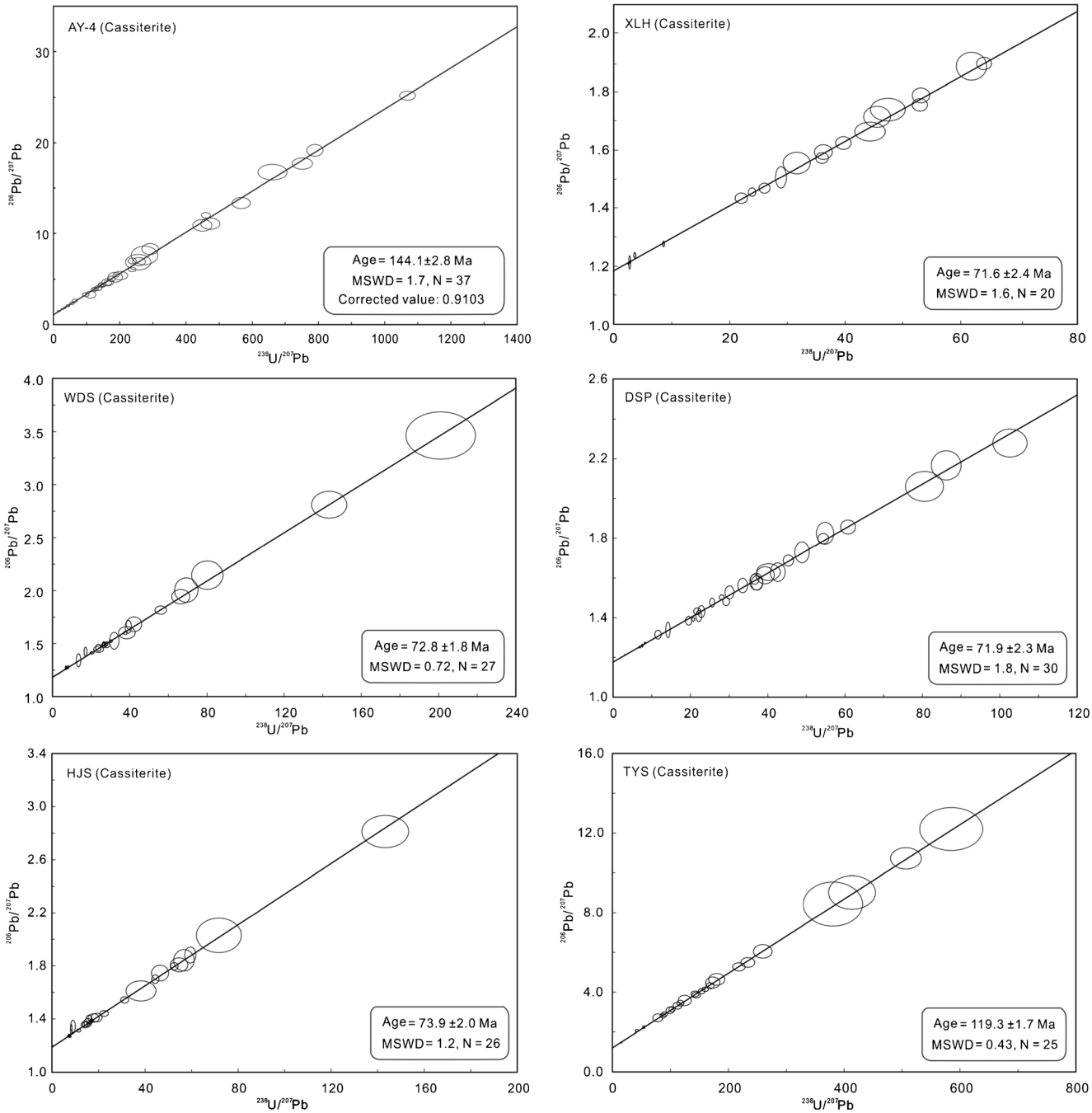

Fig. 6 $^{238}U/^{207}Pb$–$^{206}Pb/^{207}Pb$ isochron diagram for cassiterite in the samples of the second batch (XLH, WDS, DSP, and HJS from the Xiaolonghe tin deposit and TYS from the Tieyaoshan tin deposit)

122.5±0.7 Ma. The ore formation of the Lailishan tin deposit can be divided into several phases: (1) greisen, (2) skarn, and (3) quartz veins. Our data show that the quartz vein- (LLS-1) and greisen-type (LLS-2) samples yielded U/Pb ages of 47.4 ±2.0 Ma and 52.0±2.7 Ma, respectively, indicating that the different ore types of Lailishan tin deposit formed at the same time within error, although the quartz vein-type ore appears to be slightly younger, which is in agreement with the fact that the greisens are usually cut by the quartz veins. Although the ore bodies of Xiaolonghe tin deposit occur widely in space, the four ore clusters yielded U/Pb ages within a narrow range from 71.6±2.4 to 73.9±2.0 Ma. The host greisen type ore sample from the Tieyaoshan tin deposit yielded an U/Pb age of 119.3±1.7 Ma, which is in excellent agreement with the $^{40}Ar/^{39}Ar$ age of coexisting muscovite of 122.5±0.7 Ma. These tin deposits are spatially related to the Early Tertiary Lailishan granite with zircon U/Pb ages of 52.1±0.8 to 56.3 ±1.1 Ma, the Late Cretaceous Xiaolonghe granite with zircon

Table 4 Analytical data of $^{40}Ar/^{39}Ar$ step-heating dating of mica (LLS-1 from the Lailishan tin deposit, DSP from the Xiaolonghe tin deposit, and TYS from the Tieyaoshan tin deposit)

Temp (°C)		$^{40}Ar/^{39}Ar$	$^{37}Ar/^{39}Ar$	$^{36}Ar/^{39}Ar$	$^{40}Ar^*/^{39}Ar_k$	$^{40}Ar^*$ (%)	$^{39}Ar_k$ (%)	Age (Ma)	±2σ
Sample name: LLS-1 (mica); J=0.0032900±0.0000082									
750 °C		12.62167	0.02123	0.01960	6.831808	54.13	0.51	40.19	±1.02
800 °C		9.34700	0.00455	0.00506	7.851835	84.00	3.43	46.12	±0.39
840 °C		8.44703	0.00276	0.00117	8.101726	95.91	8.01	47.57	±0.25
870 °C		8.28005	0.00184	0.00040	8.160885	98.56	13.25	47.91	±0.29
900 °C	●	8.31068	0.00486	0.00030	8.221076	98.92	14.16	48.26	±0.27
920 °C	●	8.33048	0.00766	0.00039	8.215756	98.62	12.47	48.23	±0.24
940 °C	●	8.40096	0.00669	0.00056	8.236078	98.04	10.87	48.35	±0.25
960 °C	●	8.39912	0.00597	0.00040	8.280854	98.59	9.11	48.61	±0.26
990 °C	●	8.41369	0.00899	0.00041	8.293418	98.57	8.11	48.68	±0.30
1,020 °C	●	8.40792	0.02274	0.00046	8.272275	98.38	5.76	48.56	±0.33
1,060 °C	●	8.44600	0.06187	0.00068	8.249138	97.66	4.66	48.42	±0.27
1,120 °C	●	8.47494	0.13184	0.00074	8.266098	97.52	6.40	48.52	±0.28
1,180 °C	●	9.02930	0.47486	0.00278	8.250008	91.33	2.89	48.43	±0.36
1,240 °C		15.65251	0.46494	0.02348	8.753357	55.90	0.35	51.34	±1.29
Sample name: DSP (mica); J=0.0032900±0.0000082									
750 °C		19.16874	0.01364	0.02420	12.019551	62.70	1.57	70.13	±1.45
780 °C	●	14.31902	0.00077	0.00709	12.225005	85.38	7.45	71.31	±0.49
810 °C	●	13.33753	0.00132	0.00363	12.265239	91.96	8.16	71.54	±0.54
840 °C	●	13.29335	0.00276	0.00336	12.300837	92.53	8.19	71.74	±0.78
870 °C	●	13.39047	0.00081	0.00328	12.420266	92.75	10.26	72.42	±0.86
910 °C	●	13.73919	0.00144	0.00511	12.229496	89.01	13.67	71.33	±1.00
940 °C	●	14.27207	0.00087	0.00632	12.404794	86.92	12.54	72.33	±0.48
980 °C	●	14.32724	0.00098	0.00671	12.344375	86.16	22.66	71.99	±0.46
1,010 °C	●	14.03393	0.00159	0.00557	12.387150	88.27	10.24	72.23	±0.44
1,050 °C		14.79254	0.00994	0.00757	12.557901	84.89	3.25	73.21	±0.58
1,090 °C		16.12490	0.02078	0.01174	12.657973	78.50	1.01	73.78	±1.05
1,190 °C		17.24818	0.00741	0.01505	12.800394	74.21	0.99	74.59	±0.90
Sample name: TYS (mica); J=0.0037400±0.0000084									
750 °C		20.24711	0.00200	0.00994	17.308785	85.49	0.40	113.43	±1.76
800 °C		21.60960	0.00008	0.01063	18.468564	85.46	2.00	120.78	±1.09
840 °C	●	21.94041	0.00104	0.01067	18.787609	85.63	7.05	122.80	±1.03
870 °C	●	19.41071	0.00030	0.00227	18.739704	96.54	24.23	122.49	±0.79
900 °C	●	18.95566	0.00065	0.00087	18.697494	98.64	17.44	122.23	±0.84
930 °C	●	19.03113	0.00073	0.00110	18.706089	98.29	11.31	122.28	±0.75
960 °C	●	19.19449	0.00120	0.00160	18.721509	97.54	7.00	122.38	±0.86
990 °C	●	19.36242	0.00097	0.00198	18.775875	96.97	4.63	122.72	±0.72
1,030 °C	●	19.36143	0.00094	0.00219	18.713675	96.65	5.81	122.33	±0.93
1,060 °C	●	19.11855	0.00060	0.00125	18.748005	98.06	6.75	122.55	±0.91
1,090 °C	●	18.98137	0.00029	0.00072	18.769743	98.89	7.72	122.68	±1.07
1,120 °C	●	18.92818	0.00076	0.00056	18.763098	99.13	4.97	122.64	±0.75
1,160 °C		20.07825	0.00517	0.00252	19.334604	96.30	0.50	126.25	±1.53
1,260 °C		20.06088	0.03002	0.01182	16.571059	82.60	0.16	108.74	±1.47
1,300 °C		32.38111	0.06684	0.03201	22.931279	70.81	0.04	148.79	±9.22

$^{40}Ar^*$ stands for radiogenic ^{40}Ar

● means the plateau steps to calculate

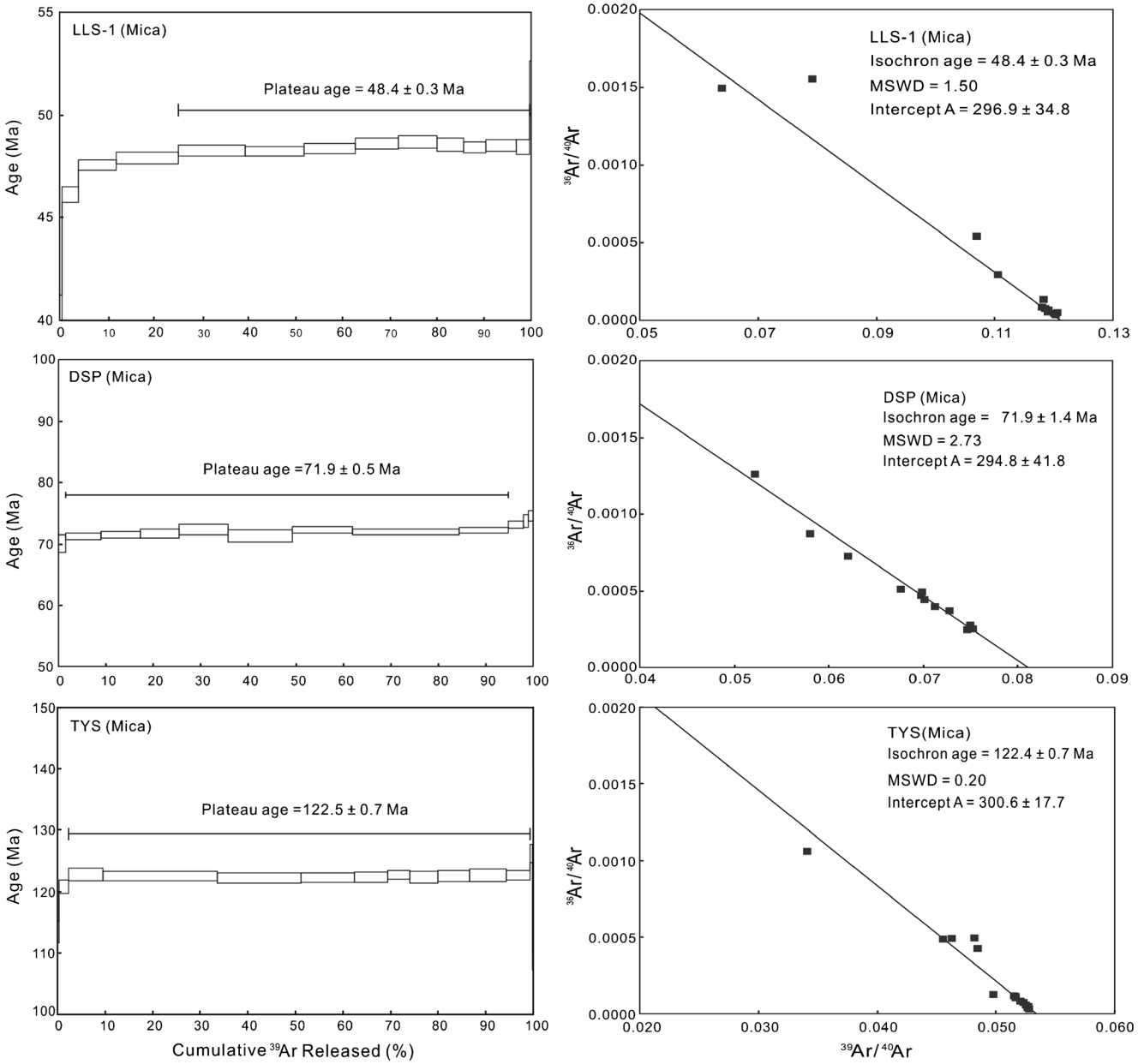

Fig. 7 $^{40}Ar/^{39}Ar$ step-heating age spectrum and isochron diagram of muscovite (LLS-1 from the Lailishan tin deposit, DSP from the Xiaolonghe tin deposit, and TYS from the Tieyaoshan tin deposit)

U/Pb ages of 67.8±1.4 to 76.0±1.0 Ma, and the Early Cretaceous Qipanshi granite with zircon U/Pb ages of 118.8 ±4.2 to 127.1±0.96 Ma, respectively. Clearly, the three tin mineralization events are contemporaneous with the emplacement of the granites (Fig. 8), which strongly supports an intrusion-related origin. The $\delta^{34}S$ values of pyrite in these deposits vary from +1.1 to +6.1‰ (Zhang 1986). They are similar to those of the spatially related granites which range from +2.8 to +5.7‰ (Shi et al. 1991), suggesting the presence of magmatic sulfur in the ore-forming fluids. The biotite granites related to tin mineralization have elevated Sn content (150 to 200 ppm) and Mg/Ti values (1.5 to 3.0) (Hou et al. 2007). The cassiterite composition with high Mg and relatively low Ti and Mn contents may also imply a genetic relation with the granite.

The relationship between tin mineralization and granitoid is well documented in the literature (Heinrich 1990; Lehmann 1990; Mao et al. 2004; Searle et al. 2012; Stemprok 1990; Taylor and Wall 1992; Zaw 1990). Tin mineralization is traditionally considered to be associated with granites rich in Sn, F, B, Li, and Cs, which generally are highly fractionated S-type granites or ilmenite-series granites. In recent years, a great deal of research has been done on the granites in the Tengchong-Lianghe tin district, and remarkable progress has been achieved. The Early Tertiary granites in which the Lailishan tin deposit occurs, the Late Cretaceous granites in

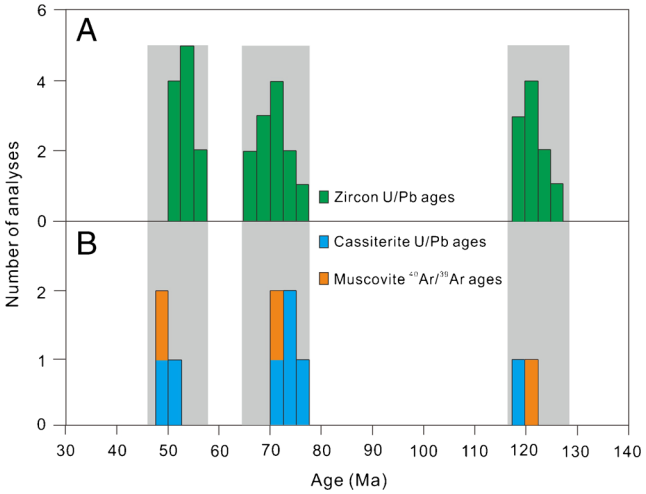

Fig. 8 Comparison of (**a**) emplacement ages of granitic rocks with (**b**) ore formation ages of tin deposits in the Tengchong-Lianghe tin district. Data for the granites are from Cong et al. (2010), Li et al. (2012a, b), Xu et al. (2011), and Yang et al. (2009)

which the Xiaolonghe tin deposit occurs, and the Early Cretaceous granites in which the Tieyaoshan tin deposit occurs show a similar mineral assemblage, with K-feldspar + plagioclase + quartz + biotite ± hornblende ± apatite. The main ferromagnesian phases are biotite. These three granite variants are highly peraluminous and characterized by abundant alkalis, volatile components (F, H_2O), LILE, and ore elements, and high initial $^{87}Sr/^{87}Sr$ ratios (0.7124–0.7138), showing S-type characteristics (Bi et al. 1992; Cong et al. 2010; Xu et al. 2011; Yang et al. 2009). However, there is an alternative view that the Late Cretaceous tin-bearing granites in the district may have A-type affinity with high Ga/Al ratios (Jiang et al. 2012).

As mentioned above, the India, Yalung Zangbo Ocean (Neo-Tethys Ocean) opened around the Middle Jurassic; its northward subduction resulted in the formation of the Gangdese magmatic arc during the Cretaceous. At ~65 Ma, the India–Eurasia collision created the Tibetan plateau. The Early and Late Cretaceous granitic magmatism and related tin metallogenesis were probably associated with the subduction of the Indian plate beneath the Eurasian plate and the Early Tertiary granite and associatied tin mineralization might be the product of postcollisional processes. This suggests that tin ore formation in the STMD could be triggered by granite magmatism in both subduction and postcollisional geodynamic setting.

Conclusions

The in situ LA-MC-ICP-MS dating of cassiterite from the Lailishan, Xiaolonghe, and Tieyaoshan tin deposits in the Tengchong-Lianghe tin district yielded well-defined $^{206}Pb/^{207}Pb$–$^{238}U/^{207}Pb$ isochron ages, which are in excellent agreement with the $^{40}Ar/^{39}Ar$ ages of coexisting muscovite in the same samples. The U/Pb ages of cassiterite and $^{40}Ar/^{39}Ar$ ages of muscovite indicate that there are three tin metallogenic events in this district: the Lailishan tin deposit at 47.4±2.0 to 52.0±2.7 Ma, the Xiaolonghe tin deposit at 71.6±2.4 to 73.9 ±2.0 Ma, and the Tieyaoshan tin deposit at 119.3±1.7 to 122.5±0.7 Ma. These ages are highly consistent with the zircon U/Pb ages of the corresponding host granites. This demonstrates that cassiterite is well suited for in situ LA-MC-ICP-MS U/Pb dating and that the tin deposits and the granites are genetically related.

Acknowledgments This work was financially supported by the State Key Program of National Natural Science Foundation of China (41130423), the CAS/SAFEA International Partnership Program for Creative Research Teams (KZZD-EW-TZ-20), and the 12th Five-Year Plan Project of the State Key Laboratory of Ore Deposit Geochemistry, Chinese Academy of Sciences (SKLODG-ZY125-03). The Yunnan Tin Industry Co. Ltd. is gratefully acknowledged for their assistance during our fieldwork. Thanks are particularly extended to the reviewers and editor Bernd Lehmann for their constructive comments and suggestions which resulted in a major improvement of this manuscript.

References

Andersen T (2002) Correction of common lead in U-Pb analyses that do not report Pb-204. Chem Geol 192:59–79

Bell K, Anglin CD, Franklin JM (1989) Sm-Nd and Rb-Sr isotope systematica of scheelites: possible implications for the age and genesis of vein-hosted gold deposits. Geology 17:500–504

Bi CS, Sheng XY, Xu QS (1992) New discovery of tin deposit related with Hercynian A-type granite in China. Sci China Ser B Chem 6: 632–638 (in Chinese)

Birch WD, Barron LM, Magee C, Sutherland FL (2007) Gold- and diamond-bearing White Hills Gravel, St Arnaud district, Victoria: age and provenance based on U-Pb dating of zircon and rutile. Aust J Earth Sci 54:609–628

Chen JC (1987) Chronology and emplacement ages of the granitic rocks in the western Yunnan. Yunnan Geol 6:101–113 (in Chinese)

Cong F, Lin SL, Xie T, Li ZH, Zou GF, Liang T (2010) Rare earth element geochemistry and U-Pb age of zircons from granites in Tengchong-Lianghe area, Western Yunnan. J Jilin Univ (Earth Sci Ed) 40:573–580, in Chinese with English abstract

Cox RA, Wilton DHC (2006) U-Pb dating of perovskite by LA-ICP-MS: an example from the Oka carbonatite, Quebec, Canada. Chem Geol 235:21–32

Cui YR, Zhou HY, Geng JZ, Li HK, Li HM (2012) In situ LA-MC-ICP-MS U-Pb isotopic dating of monazite. Acta Geosci Sin 33:865–876, in Chinese with English abstract

Gulson BL, Jones MT (1992) Cassiterite: potential for direct dating of mineral deposits and a precise age for the Bushveld complex granites. Geology 20:355–358

Heinrich CA (1990) The chemistry of hydrothermal tin(-tungsten) ore deposition. Econ Geol 85:457–481

Horn I, Rudnick RL, McDonough WF (2000) Precise elemental and isotope ratio determination by simultaneous solution nebulization and laser ablation-ICP-MS: application to U-Pb geochronology. Chem Geol 164:281–301

Horstwood MSA, Foster GL, Parrish RR, Noble SR, Nowell GM (2003) Common-Pb corrected in situ U-Pb accessory mineral geochronology by LA-MC-ICP-MS. J Anal At Spectrom 18: 837–846

Hou ZQ, Zaw K, Pan GT, Mo XX, Xu Q, Hu YZ, Li XZ (2007) Sanjiang Tethyan metallogenesis in SW China: tectonic setting, metallogenic epochs and deposit types. Ore Geol Rev 31:48–87

Jiang BA, Gong QJ, Zhang J, Ma N (2012) Late cretaceous aluminium A-type granites and its geological significance of Dasongpo Sn deposit, Tengchong, West Yunnan. Acta Petrol Sin 28:1477–1492, in Chinese with English abstract

Kempe U, Belyatsky BV, Krymsky RS, Kremenetsky AA, Ivanov PA (2001) Sm-Nd and Sr isotope systematics of scheelite from the giant Au(-W) deposit Muruntau (Uzbekistan): implications for the age and sources of Au mineralization. Miner Deposita 36:379–392

Kooijman E, Mezger K, Berndt J (2010) Constraints on the U-Pb systematics of metamorphic rutile from in situ LA-ICP-MS analysis. Earth Planet Sci Lett 293:321–330

Lehmann B (1990) Metallogeny of tin. Springer, Berlin, 211 p

Li QL, Li SG, Zheng YF, Li HM, Massonne HJ, Wang QC (2003) A high precision U-Pb age of metamorphic rutile in coesite-bearing eclogite from the Dabie Mountains in central China: a new constraint on the cooling history. Chem Geol 200:255–265

Li JW, Deng XD, Zhou MF, Lin YS, Zhao XF, Guo JL (2010) Laser ablation ICP-MS titanite U-Th-Pb dating of hydrothermal ore deposits: a case study of the Tonglushan Cu-Fe-Au skarn deposit, SE Hubei Province, China. Chem Geol 270:56–67

Li ZH, Lin SL, Cong F, Zou GF, Xie T (2012a) Early Cretaceous magmatism in Tengchong-Lianghe block, western Yunnan. Bull Mineral Petrol Geochem 31:590–598, in Chinese with English abstract

Li ZH, Lin SL, Cong F, Zou GF, Xie T (2012b) U-Pb dating and Hf isotopic compositions of quartz diorite and monzonitic granite from the Tengchong-Lianghe block, western Yunnan, and its geological implications. Acta Geosci Sin 86:1047–1062, in Chinese with English abstract

Li KW, Zhang Q, Wang DP, Cai Y, Liu YP (2013) LA-MC-ICP-MS U-Pb geochronology of cassiterite from the Bainiuchang polymetallic deposit, Yunnan Province, China. Acta Miner Sin 33:523–529, in Chinese with English abstract

Liu GL, Qin DX, Fan ZG (2005) Tin resource and its sustainable developing in Yunnan Province. Conservation and Utilization of Mineral Resources, 2:9–13 (in Chinese)

Liu YP, Li ZX, Li HM, Guo LG, Xu W, Ye L, Li CY, Pi DH (2007) U-Pb geochronology of cassiterite and zircon from the Dulong Sn-Zn deposit: evidence for cretaceous large-scale granitic magmatism and mineralization events in southeastern Yunnan province, China. Acta Petrol Sin 23:967–976, in Chinese with English abstract

Ludwig KR (1997) Isoplot—a plotting and regression program for radiogenic-isotope data. USGS Open-file report, version 2:92

Ludwig KR (2001) Users manual for Isoplot/Ex: a geochronological toolkit for Microsoft Excel. Berkeley Geochronology Center Special Publication, 19 pp

Mao JW, Zhang ZC, Zhang ZH, Du AD (1999) Re-Os isotopic dating of molybdenites in the Xiaoliugou W (Mo) deposit in the northern Qilian mountains and its geological significance. Geochim Cosmochim Acta 63:1815–1818

Mao JW, Li XF, Chen W, Lan XM, Wei SL (2004) $^{40}Ar/^{39}Ar$ dating of tin ores and related granite in Furong tin ore field Hunan Province, and its geodynamic significance. Miner Depos 23:164–175, in Chinese with English abstract

Mao JW, Wang YT, Lehmann B, Yu JJ, Ad D, Mei YX, Li YF, Zang WS, Stein HJ, Zhou TF (2006) Molybdenite Re–Os and albite $^{40}Ar/^{39}Ar$ dating of Cu–Au–Mo and magnetite porphyry systems in the Yangtze River valley and metallogenic implications. Ore Geol Rev 29:307–324

Mo XX, Niu YL, Dong GC, Zhao ZD, Hou ZQ, Zhou S, Ke S (2008) Contribution of syncollisional felsic magmatism to continental crust growth: A case study of the Paleogene Linzizong volcanic Succession in southern Tibet. Chem Geol 250:49–67

Peng MS, He SM (1985) A spectroscopic study of cassiterite from different genesis. Chin Sci Bull 8:600–603 (in Chinese)

Peng JT, Hu RZ, Burnard PG (2003) Samarium-neodymium isotope systematics of hydrothermal calcites from the Xikuangshan antimony deposit (Hunan, China): the potential of calcite as a geochronometer. Chem Geol 200:129–136

Peng JT, Hu RZ, Bi XW, Dai TM, Li ZL, Li XM, Shuang Y, Yuan SD, Liu SR (2007) $^{40}Ar/^{39}Ar$ isotopic dating of tin mineralization in Furong deposit of Hunan Province and its geological significance. Miner Depos 26:237–248, in Chinese with English abstract

Schandl ES, Davis DW, Krogh TE (1990) Are the alteration halos of massive sulfide deposits syngenetic? Evidence from U-Pb dating of hydrothermal rutile at the Kidd Volcanic Center, Abitibi subprovince, Canada. Geology 18:505–508

Schmidberger SS, Heaman LM, Simonetti A, Creaser RA, Cookenboo HO (2005) Formation of Paleoproterozoic eclogitic mantle, Slave Province (Canada): insights from in-situ Hf and U-Pb isotopic analyses of mantle zircons. Earth Planet Sci Lett 240:621–633

Searle MP, Whitehouse MJ, Robb LJ, Ghani AA, Hutchison CS, Sone M, Ng SWP, Roselee MH, Chung SL, Oliver GJH (2012) Tectonic evolution of the Sibumasu-Indochina terrane collision zone in Thailand and Malaysia: constraints from new U-Pb zircon chronology of SE Asian tin granitoids. J Geol Soc Lond 169:489–500

Shi L, Tang LD, Zhao M, Zhang WP (1991) Types of primary tin ore deposit and metallogenic mechanism in Tengchong-Lianghe area. Yunnan Geol 10:191–322, in Chinese

Shi RD, Yang JS, Xu ZQ, Qi XX (2008) The Bangong Lake ophiolite (NW Tibet) and its bearing on the tectonic evolution of the Bangong–Nujiang suture zone. J Asian Earth Sci 32:438–457

Simonetti A, Neal CR (2010) In-situ chemical, U-Pb dating, and Hf isotope investigation of megacrystic zircons, Malaita (Solomon Islands): evidence for multi-stage alkaline magmatic activity beneath the Ontong Java Plateau. Earth Planet Sci Lett 295:251–261

Simonetti A, Heaman LM, Chacko T, Banerjee NR (2006) In situ petrographic thin section U-Pb dating of zircon, monazite, and titanite using laser ablation-MC-ICP-MS. Int J Mass Spectrom 253:87–97

Smith M, Storey C, Jeffries T (2005) LA-ICPMS U-Pb dating of titanite: new constraints on multistage geological evolution of the Norrbotten mining district, Sweden. Miner Depos Res Meet Glob Chall 1:829–832

Steiger RH, Jäger E (1977) Subcommission on geochronology: convention on the use of decay constants in geo- and cosmochronology. Earth Planet Sci Lett 36:359–362

Stein HJ, Markey RJ, Morgan JW, Hannah JL, Schersten A (2001) The remarkable Re-Os chronometer in molybdenite: how and why it works. Terra Nova 13:479–486

Stemprok M (1990) Solubility of tin, tungsten and molybenum oxides in felsic magmas. Miner Deposita 25:205–212

Storey CD, Smith MP, Jeffries TE (2007) In situ LA-ICP-MS U-Pb dating of metavolcanics of Norrbotten, Sweden: records of extended geological histories in complex titanite grains. Chem Geol 240:163–181

Tang L (1992) Discussion to genetic type of Lailishan tin deposit in Tengchong-Lianghe region. Yunnan Geol 11:283–288, in Chinese

Taylor JR, Wall VJ (1992) The behavior of tin in granitoid magmas. Econ Geol 87:403–420

Valeriano CD, Tupinamba M, Simonetti A, Heilbron M, Almeida JCH, Eirado LG (2011) U-Pb LA-MC-ICPMS geochronology of Cambro-Ordovician post-collisional granites of the Ribeira belt, southeast Brazil: terminal Brasiliano magmatism in central Gondwana supercontinent. J S Am Earth Sci 32:416–428

Wang F, Zhou XH, Zhang LC, Ying JF, Zhang YT, Wu FY, Zhu RX (2006) Late Mesozoic volcanism in the Great Xing'an range (NE China): timing and implications for the dynamic setting of NE Asia. Earth Planet Sci Lett 251:179–198

Willigers BJA, Baker JA, Krogstad EJ, Peate DW (2002) Precise and accurate in situ Pb-Pb dating of apatite, monazite, and sphene by laser ablation multiple-collector ICP-MS. Geochim Cosmochim Acta 66:1051–1066

Wu FY, Yang YH, Marks MAW, Liu ZC, Zhou Q, Ge WC, Yang JS, Zhao ZF, Mitchell RH, Markl G (2010) In situ U-Pb, Sr, Nd and Hf isotopic analysis of eudialyte by LA-(MC)-ICP-MS. Chem Geol 273:8–34

Xu H, Zhang MH, Zhu SZ (2010) An approach to geological features and genesis for the Lianghe tin deposit. Acta Geol Sin 30:206–209, in Chinese with English abstract

Xu YG, Yang QJ, Lan JB, Luo ZY, Huang XL, Shi YR, Xie LW (2011) Temporal-spatial distribution and tectonic implications of the batholiths in the Gaoligong-Tengliang-Yingjiang area, western Yunnan: constraints from zircon U-Pb ages and Hf isotopes. J Asian Earth Sci 53:151–175

Yang QJ, Xu YG, Huang XL, Luo ZY, Shi YR (2009) Geochronology and geochemistry of granites in the Tengliang area, western Yunnan: tectonic implication. Acta Petrol Sin 25:1092–1104, in Chinese with English abstract

Yin A, Harrison TM (2000) Geologic evolution of the Himalayan-Tibetan orogen. Annu Rev Earth Pl Sc 28:211–280

Yuan SD, Peng JT, Hu RZ, Li HM, Shen NP, Zhang DL (2008) A precise U-Pb age on cassiterite from the Xianghualing tin-polymetallic deposit (Hunan, South China). Miner Deposita 43:375–382

Yuan SD, Peng JT, Hao S, Li HM, Geng JZ, Zhang DL (2011) In situ LA-MC-ICP-MS and ID-TIMS U-Pb geochronology of cassiterite in the giant Furong tin deposit, Hunan Province, South China: new constraints on the timing of tin-polymetallic mineralization. Ore Geol Rev 43:235–242

Yuan SD, Zhang DL, Shuang Y, Du AD, Qu WJ (2012) Re-Os dating of molybdenite from the Xintianling giant tungsten-molybdenum deposit in southern Hunan Province, China and its geological implications. Acta Petrol Sin 28:27–38, in Chinese with English abstract

Zack T, Stockli DF, Luvizotto G, Barth MG, Belousova E, Wolfe MR, Hinton RW (2011) In situ U-Pb rutile dating by LA-ICP-MS: Pb-208 correction and prospects for geological applications. Contrib Mineral Petrol 162:515–530

Zaw K (1990) Geological, petrogical and geochemical characteristics of granitoid rocks in Burma: with special reference to the associated W-Sn mineralization and their tectonic setting. J SE Asian Earth Sci 4: 293–335

Zhang SL (1986) Geological setting and ore types of the Tengchong tin ore belt in Yunnan province. Miner Depos 5: 19–26, in Chinese

Zhang LS, Schärer U (1996) Inherited Pb components in magmatic titanite and their consequence for the interpretation of U-Pb ages. Earth Planet Sci Lett 138:57–65

Zhang DL, Peng JT, Hu RZ, Yuan SD, Zheng DS (2011) The closure of U-Pb isotope system in cassiterite and its reliability for dating. Geol Rev 57:549–554, in Chinese with English abstract

Zhou HY, Geng JZ, Cui YR, Li HK, Li HM (2012) In situ U-Pb dating of apatite using LA-MC-ICP-MS. Acta Geosci Sin 33:857–864, in Chinese with English abstract

Zhou HY, Li HM (2008) The improvement of the rutile isotope dilution U-Pb dating methodology. Acta Petrologica et Mineralogica 27:77–80